MACE Silicon Nanostructures

Ciro Chiappini

Contents

Introduction 172
Morphology of Nanostructures 173
  Effect of Oxidizers 174
  Effect of Metal 176
  Effect of Substrate 179
  Effect of Other Parameters 180
Etch Rate 181
Properties of MACE Porous Nanowires 182
References 184

Abstract

Metal-assisted chemical etching (MACE) of silicon is receiving much interest as a controllable method of generating silicon nanostructures of varied forms, including porous silicon. The various morphologies, etch chemistry variables (e.g., metal catalysts, substrate type, electrolyte temperature), and potential applications of the resulting nanostructures are reviewed.

Kim et al. (2011), Geyer et al. (2012), Chiappini et al. (2010), Chartier et al. (2008), Li and Bohn (2000), Dudley and Kolasinski (2009), Peng et al. (2003, 2006), Yae et al. (2007) of particular interest.

C. Chiappini (✉)
Department of Materials, Imperial College London, Faculty of Engineering, London, UK
e-mail: ciro.chiappini@gmail.com

© Springer International Publishing Switzerland 2014

L. Canham (ed.), *Handbook of Porous Silicon*,
DOI 10.1007/978-3-319-05744-6_17

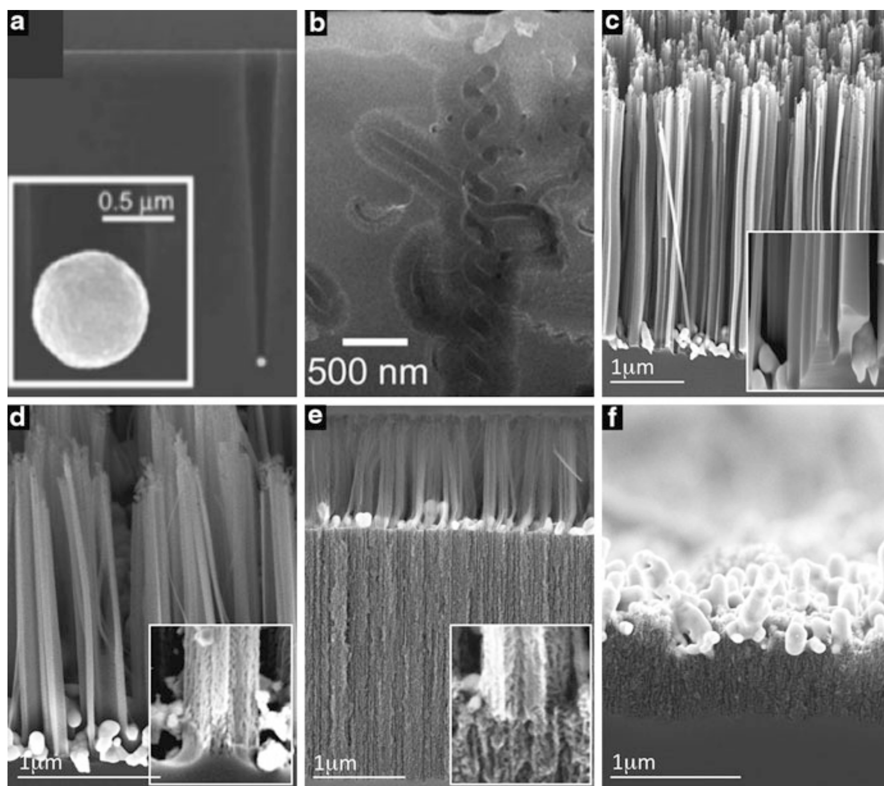

Fig. 1 Overview of nanostructures synthesized by metal-assisted chemical etch. (**a**) Nanopores with solid sidewalls (sNPs), from Lee et al. (2008); (**b**) nanopores with mesoporous sidewalls (mNPs), from Tsujino et al. (2005); (**c**) solid nanowires (sNWs), from Chiappini et al. (2010); (**d**) mesoporous nanowires (mNWs), from Chiappini et al. (2010); (**e**) porous nanowires over porous silicon, from Chiappini et al. (2010); (**f**) porous silicon (pSi), from Chiappini et al. (2010)

Introduction

The formation of porous silicon by metal-assisted chemical etch (MACE) was discovered in 1997 when patterned aluminum on silicon rapidly induced selective formation of porous silicon layers in stain-etch conditions (Dimova-Malinovska et al. 1997).

In a typical MACE process, a patterned metal deposited over a silicon substrate catalyzes etch of silicon in its vicinities, when placed in an oxidizing solution of hydrofluoric acid (HF). By anisotropically etching silicon in the vicinity of a metal mask, MACE generates silicon structures dictated by metal patterning and etching conditions: pores, nanowires, and porous silicon layers (Fig. 1). MACE combined with lithographic patterning generates high aspect ratio silicon nanostructures of tailored geometry (Kim et al. 2011a; Geyer et al. 2012; Chiappini et al. 2010; Wang et al. 2012; Mikhael et al. 2011).

Under appropriate MACE conditions, porous silicon forms in the un-etched silicon around the metal (Geyer et al. 2012; Chiappini et al. 2010; Tsujino and Matsumura 2005; Chartier et al. 2008). Combining anisotropic etching and porosification, MACE is a simple strategy to form high aspect ratio porous silicon nanostructures. MACE is a top-down nanofabrication technique that allows finer control than competing bottom-up strategies for growth of silicon nanowires. MACE provides highly crystalline nanowires and grants control over their doping, surface roughness, and porosity. MACE is a low-cost strategy, which works at ambient temperature and pressure, to reproducibly generate wafer-scale porous silicon as well as ordered arrays of oriented nanowires, nanorods, and vias (see complementary handbook chapters "▶ Porous Silicon Formation by Metal Nanoparticle-Assisted Etching," "▶ Porous Silicon Formation by Galvanic Etching," and "▶ Porous Silicon Formation by Stain Etching").

There are good arguments to support that MACE and stain etching are two tightly correlated manifestations of the same process. Both techniques rely on the underlying principle that hole injection from an oxidizer in solution induces silicon oxidation (Chartier et al. 2008; Kolasinski 2005; Li and Bohn 2000). The most recent advances in stain etching show that oxidants containing metal ions induce a faster and more reproducible etch that generates thick porous silicon films of higher quality than the traditional etchants (Nahidi and Kolasinski 2006; Dudley and Kolasinski 2009; Loni et al. 2011). On the other hand, MACE can form porous and solid silicon nanowires in solutions containing only HF and metal ion oxidizing salts without any pre-deposition of metal (Hochbaum et al. 2009; Peng et al. 2003).

This chapter aims to condense the current knowledge of MACE into a set of empirical guidelines for the rational design of MACE nanostructures. The effects of known MACE parameters on the resulting structure will be presented. Finally, a summary of the known properties of MACE nanostructures will be outlined.

Morphology of Nanostructures

Metal-assisted chemical etch is employed to form a wide range of silicon structures, including nanopores, i.e., pores of submicron size, with either solid sidewalls (Dimova-Malinovska et al. 1997; Tsujino and Matsumura 2005, 2007; Chartier et al. 2008) (sNP, Fig. 1a) or mesoporous sidewalls (Dimova-Malinovska et al. 1997; Tsujino and Matsumura 2005, 2007; Chartier et al. 2008) (mNPs, Fig. 1b), porous silicon layers (Dimova-Malinovska et al. 1997; Kim et al. 2011a; Chiappini et al. 2010; Mikhael et al. 2011; Chartier et al. 2008; Voigt et al. 2011) (pSi, Fig. 1c), solid nanowires (Chiappini et al. 2010; Chartier et al. 2008; Peng et al. 2003; Huang et al. 2010a) (sNWs, Fig. 1d), mesoporous nanowires (Chiappini et al. 2010; Chartier et al. 2008; Hochbaum et al. 2009; Chen et al. 2010a) (mNWs, Fig. 1e), porous nanowires over porous silicon (Fig. 1f), and polished surfaces (Chiappini et al. 2010; Chartier et al. 2008; Nahidi and Kolasinski 2006; Dudley and Kolasinski 2009) (PS). The following sections will explore the effect of some crucial MACE parameters on the resulting nanostructures.

Table 1 Common oxidizers for MACE, their associated cathode reaction, and the MACE structures they have been employed to form

Oxidizer	Cathode reaction	Structures	References
H_2O_2	$H_2O_2 + 2H^+ \rightarrow 2H_2O + 2h^+$	sNP, mNP, pSi, sNW, mNW, PS	Tsujino and Matsumura (2007), Megouda et al. (2009), Zhang et al. (2009)
	$2H^+ \rightarrow H_2^g + 2h^+$		Chartier et al. (2008), Li and Bohn (2000), Peng et al. (2006a)
HNO_3	$HNO_3 + 3H^+ \rightarrow NO + 2H_2O + 3h^+$	sNP, pSi	Dimova-Malinovska et al. (1997)
Metal salt (M^{n+})	$M^{m+} \rightarrow M^{(m-n)+} + nh^+$	pSi, sNW, mNW	Nahidi and Kolasinski (2006), Dudley and Kolasinski (2009)
	Metal ions can be neutralized (M^0) and precipitated		

Effect of Oxidizers

The solution-metal-silicon system constitutes a microscopic electrochemical cell that induces anodic silicon etch. For the most commonly employed oxidants H_2O_2 and HNO_3, the proposed cathodic reactions provide free positive carriers to be transferred to the silicon (Table 1).

In the anode reaction, the silicon consumes the positive carriers and is solubilized through oxidation. Several models for the anodic reactions have been proposed and are outlined in the handbook chapter "▶ Porous Silicon Formation by Metal Nanoparticle-Assisted Etching."

A wide variety of metal salts can induce silicon porosification without the addition of any other oxidizer, as their electrochemical potential is sufficiently high to directly inject holes in the valence band of silicon. Those that have been employed for MACE are listed in the following table alongside the nanostructures they have been shown to produce (Table 2).

All oxidizers have a standard energy sufficient to inject holes into the valence silicon, and the metal deposited on the silicon surface is not necessary for the dissolution to occur. The metal acts as a catalyst facilitating charge transfer between the silicon and the oxidizers in solution. As a consequence, etching occurs preferentially in the vicinity of the metal due to the higher concentration of free holes.

Hydrogen Peroxide

Hydrogen peroxide is by far the most commonly employed oxidizer in MACE. Chartier et al. assume that the relative concentration of HF and H_2O_2 in a MACE etch solution plays a similar role to J_{ps} in anodic etch (Chartier et al. 2008). To this extent, they define a useful parameter to correlate the relative concentrations of HF and H_2O_2 in solution with the resulting silicon structures:

$$\rho = \frac{[HF]}{[HF] + [H_2O_2]}$$

Table 2 Metal-based oxidizers employed in MACE and resulting MACE structures

Oxidizer	MACE structures	References
$AgNO_3$	pSi, sNW, mNW	Hochbaum et al. (2009), Peng et al. (2003), Chen et al. (2010a), Zhang et al. (2009), Peng et al. (2006a), Yae et al. (2003), Chen et al. (2008, 2010b), Sivakov et al. (2009), Zhu et al. (2011)
AgO	pSi, sNW, mNW	Kato and Adachi (2011)
$HAuCl_4$	NW, sNP, mNP	Yae et al. (2005, 2007), Peng and Zhu (2004, 2003)
$KAuCl_4$		
H_2PtCl_6	sNP, mNP, pSi	Peng et al. (2003), Yae et al. (2005)
K_2PtCl_6		
$PdCl_2$	sNP, mNP, pSi	Yae et al. (2005)
$Na_2S_2O_8$	sNP, mNP, pSi	Douani et al. (2008)
$K_2Cr_2O_7$	sNP, mNP, pSi	Douani et al. (2008)
$KMnO_4$ $NaMnO_4$	sNP, mNP, pSi	Douani et al. (2008)
$Fe(NO_3)_3$	sNP, sNW, mNW, pSi	Peng et al. (2006b)
$FeCl_3$	pSi	Nahidi and Kolasinski (2006), Dudley and Kolasinski (2009), Loni et al. (2011)
V_2O_5	pSi	Dudley and Kolasinski (2009)
CeF_4	pSi	Dudley and Kolasinski (2009)
$M(NO_3)_2$ M = Ni, Mn, Cu, Fe, Co, Cr, Mg	sNP, pSi, sNW, mNW	Peng et al. (2003)

It was observed that structures transition from solid etches (sNPs, sNWs) to mesoporous etches (mNPs, mNWs, pSi) to polished surfaces with decreasing ρ, id est with increasing relative concentration of H_2O_2 (Chiappini et al. 2010; Chartier et al. 2008). Figure 2 plots a collection of 108 etch conditions sourced from 13 independent publications, where silicon substrates deposited with Ag from $AgNO_3$ solution in HF were etched in $HF/H_2O_2/H_2O$ solution at room temperature, in the absence of any other solvent (Geyer et al. 2012; Chiappini et al. 2010; Tsujino and Matsumura 2005; Chartier et al. 2008; Huang et al. 2010a; Zhang et al. 2008, 2009; Zhong et al. 2011; Wu et al. 2012a, b; Wang et al. 2011; Qu et al. 2010; Sivakov et al. 2010). Etch time was not a considered parameter. Substrate-doping type does not seem to play a significant role in the resulting structures. Albeit substrates of different resistivity have different transition thresholds, decreasing ρ induces porosification first and polishing then. As the oxidizer concentration is

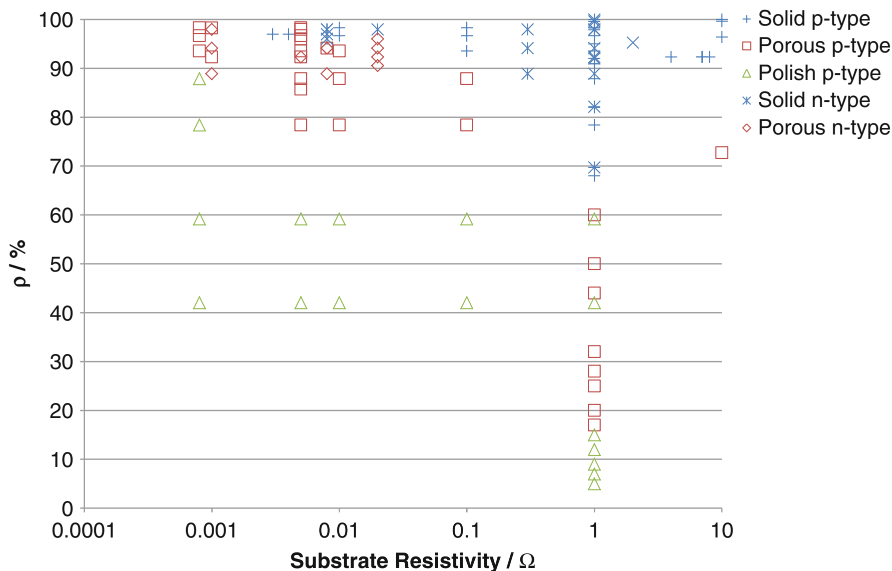

Fig. 2 Phase diagram for the nanostructures resulting from MACE as a function of substrate resitivity and the ρ parameter. Collection of 108 experiments from 13 independent publications. Solid indicates pores with either solid sidewalls or solid nanowires; porous indicates pores with either mesoporous sidewalls, mesoporous nanowires, or porous silicon; polish indicates complete surface polishing

ultimately responsible for the rate of hole injection, and thus of the anodic current, it is expected that increasing oxidizer concentration would lead to more porosification, larger pores with higher porosity, and eventually surface polishing. The data available to estimate pore size and porosity is significantly scarcer but supports the idea of larger pores and increasing porosity with decreasing ρ (Chiappini et al. 2010; Zhong et al. 2011; Wang et al. 2011; Qu et al. 2010).

By tuning the concentration of oxidant in solution over time, it is possible to obtain mesoporous nanowires and nanopores with segments of different porosity (Chiappini et al. 2010; Chartier et al. 2008; Kolasinski 2005), as well as nanostructures with segments of different orientation, switching periodically from 100 to non-100 (zigzag) (Refer to sections "Orientation" and "Etch Rate").

Effect of Metal

A wide range of transition metals can catalyze MACE. Noble metals are especially favored for the formation of nanowires as well as for nanostructures with defined cross sections since they better preserve their structure during the etch, as they do not dissolve in HF. Non-noble transition metals have been mostly used to form sNP, pSi, and polished surfaces. Metals can be deposited on Si by a variety of methods, including electroless deposition (Peng et al. 2003; Peng and Zhu 2004;

Table 3 Morphology of metal deposition, associated deposition techniques, and resulting MACE structures

Metal morphology	Deposition	MACE structures	References
Continuous film	Sputtering	pSi	Dimova-Malinovska et al. (1997), Geyer et al. (2012), Peng et al. (2003)
	Evaporation		
	Electroplating		
	Electroless		
Patterned film	Evaporation	Tailored structures	Kim et al. (2011a), Geyer et al. (2012), Chiappini et al. (2010), Mikhael et al. (2011), Balasundaram et al. (2012)
	Sputtering		
	Electroless		
Discontinuous film	Evaporation	pSi, sNW, mNW, PS	Megouda et al. (2009), Peng and Zhu (2004), Yae et al. 2007, Peng et al. (2006b)
	Sputtering		
	Electroless		
Dendrites	Electroless	pSi, sNW, mNW, PS	Chiappini et al. (2010), Chartier et al. (2008), Peng et al. (2003, 2006b), Peng and Zhu (2004), (Sivakov)
Nanoparticles	Electroless	sNP, mNP, pSi, PS	Dimova-Malinovska et al. (1997), Tsujino and Matsumura (2005), Chartier et al. (2008), Lee et al. (2008), Yae et al. (2007)
	From solution		
	Electroplating		

Yae et al. 2007), electroplating (Yae et al. 2005) evaporation (Dimova-Malinovska et al. 1997; Chiappini et al. 2010; Zhong et al. 2011; Weisse et al. 2012), sputtering, focused ion beam-assisted deposition, and nanoparticle deposition from solution (Lee et al. 2008; Harada et al. 2001). Each deposition strategy can generate specific metal morphologies, which best suits specific MACE structures (Table 3).

Continuous metal films that extend over several tens of microns tend not to sink into the silicon and are unable to form MACE nanostructures, at time impeding MACE altogether as they prevent the silicon underneath from interacting with the solution. In appropriate conditions, silicon porosification can occur underneath and in the vicinity of extended metal films (Geyer et al. 2012).

A common strategy is to pattern metal films by nanosphere lithography combined with metal evaporation to obtain nanoscale-size hexagonally close-packed dot arrays (Mikhael et al. 2011). The arrays of dots then undergo MACE to form solid or porous silicon nanopillars. This general strategy can be extended to any lithographic technique to obtain porous silicon nanostructures of tailored geometry (Kim et al. 2011a, b; Harada et al. 2001). Multiple layers of different metals (e.g., Au/Ag) are employed to improve Ag stability in oxidizing conditions and allow for extended etch of high aspect ratio structures (Kim et al. 2011a).

MACE of tailored nanostructure occurs also by combining lithographic patterning with electroless deposition, with the assistance of a hard, HF-resistant mask, such as polystyrene or low-stress silicon nitride (Chiappini et al. 2010; Asoh et al. 2009).

Table 4 Metal salts precursors for electroless deposition and resulting metal morphology

Metal	Precursor	Morphology	References
Ag	$AgNO_3$	Nanoparticles	Chiappini et al. (2010), Chartier et al. (2008), Hochbaum et al. (2009), Peng et al. (2003, 2006a)
		Dendrites	
Au	$HAuCl_4$	Nanoparticles	Chiappini et al. (2010), Megouda et al. (2009), Yae et al. (2005), Peng and Zhu (2003)
		Dendrites	
	$KAuCl_4$	Films	
Pt	H_2PtCl_6	Nanoparticles	Yae et al. (2003), Peng et al. (2005, 2006b)
	K_2PtCl_6	Films	
Pd	$PdCl_2$	Nanoparticles	Yae et al. (2005, 2007)
		Films	
Cu	$Cu(NO_3)_2$	Nanoparticles	Peng et al. (2003, 2006b)
		Films	

Discontinuous metal films produce thin silicon nanowires, which can be mesoporous or solid (Peng et al. 2006b). They are also employed to form porous silicon or electropolished surfaces (Peng and Zhu 2004).

Dendrites form during extended electroless deposition of Ag or Au and are the most commonly employed strategy to form dense forests of aligned silicon nanowires or nanoplatelets. Tuning MACE conditions it is possible to obtain pSi or PS from dendrites (Chiappini et al. 2010).

Isolated metal nanoparticles yield nanopores, which can have solid or mesoporous sidewalls. Similarly as for dendrites, the conditions can be tuned to form pSi or PS (Tsujino and Matsumura 2005; Chartier et al. 2008; Lee et al. 2008; Yae et al. 2007).

Electroless deposition (ELD) of noble metals on the silicon surface is widely employed in MACE. By ELD metal ions from a precursor salt in a solution of HF inject holes in the silicon valence band and as a result get reduced and nucleate on the silicon surface. This process is by no means different than MACE, and in fact during ELD, the substrate gets also etched. ELD is a very simple and versatile strategy that yields a wide array of metal morphologies, albeit with more limited control with respect to the alternatives. ELD of noble metals generates all morphologies ranging from isolated nanoparticles to continuous metal films, but with limited control on nanoparticle size, arrangement, metal film thickness and uniformity, grain, and domain size. Not all electroless deposited metals can achieve all structures (Table 4).

Deposition time and precursor concentration can control the resulting metal morphology (Peng and Zhu 2004; Yae et al. 2007). Initially, metal nanoparticles nucleate on the silicon surface. As time progresses, the nanoparticles grow in size eventually becoming dendrites or metal films (initially discontinuous and then continuous) (Chartier et al. 2008; Peng et al. 2003; Yae et al. 2003). The density of nanoparticles depends on the metal employed, its concentration, and the state of the silicon surface (Yae et al. 2007).

Table 5 Etch direction as a function of substrate orientation and etching rate

Etch direction	<100>	<110>	<111>	Other
Substrate orientation				
(100)	All but extremely high etch rate	Extremely high etch rate	X	X
(110)	Low etch rate	High etch rate	X	Zigzag etch
(111)	Low etch rate	X	High etch rate	Zigzag or <113> etch

Effect of Substrate

Doping

Within the variety of etch conditions explored in the literature, MACE has shown little dependence on substrate-doping type (Fig. 2). n-type (30 occurrences) and p-type (78 occurrences) silicon start porosifying and polishing at comparable values of ρ. The resulting porous structures for p- and n-type silicon are also similar. This behavior is justified in contrast to what is observed for electrochemical etch; as for MACE, the positive carriers necessary for the oxidation are supplied from the solution and do not originate from the semiconductor.

Doping concentration instead plays an important role controlling the etch morphology (Chiappini et al. 2010; Mikhael et al. 2011; Zhong et al. 2011). For all resistivities considered, both solid and mesoporous structures can arise for Ag-deposited substrate etched in H_2O_2/HF (Fig. 2; Chiappini et al. 2010; Chen et al. 2010a; Bai et al. 2012). Polishing could also be obtained for any substrate in appropriate conditions (Chiappini et al. 2010). Limited data is available for other metal catalysts, but it suggests a similar behavior at least for Au and Pt. Choosing appropriate values of ρ, with decreasing resistivity, the etch morphology can transition from solid to mesoporous to polished. When forming porous structures, decreasing substrate resistivity is correlated with increased surface area and average pore size.

Orientation

The available data suggests that at low etch rates, there is a preferential etch in the <100> direction regardless of substrate orientation (Kim et al. 2011a; Huang et al. 2010a; Chen et al. 2008, 2010b; Wu et al. 2012a; Sivakov et al. 2010). As the etch rate increases in non-(100) substrates, the etch orients in the vertical direction. In some instances, a progressive orientation occurs. This phenomenon has been justified through the energy requirements for silicon backbond breaking, in analogy to the descriptions of electrochemical etch and anisotropic silicon etch in alkaline conditions. Lower etch rates are associated with lower hole injection rates, which in turn induce a preferential etch in the <100> direction as only two backbonds must be broken for the etch to progress. Kim et al. observed <110> etch in (100) substrates for extremely high etch rates surpassing 1,500 nm/min (Kim et al. 2011a) and suggested a correlation between etch rate and etch orientation. This phenomenon was also interpreted in terms of backbond breaking energies (Table 5).

The etch rate, which determines orientation, is controlled by multiple parameters during MACE and will be discussed in detail in section "Etch Rate" (Kim et al. 2011a). Typically etch orientation is controlled by tuning the concentration of oxidizer (H_2O_2) in solution or the temperature. In general, higher H_2O_2 concentrations and higher temperatures are conducive to higher etch rates.

By appropriately controlling the etch conditions, it is possible to obtain both solid and mesoporous nanowires for all orientations. By alternating between regimes of high and low etch rate during MACE, it is possible to form zigzag pores or zigzag wires, both solid and mesoporous (Chen et al. 2010b; Wu et al. 2012a; Sivakov et al. 2010). Addition of organic solvents also influences the etch directionality. Addition of ethanol or methanol to the etch solution resulted in slanted nanopillars, while 2-propanol and acetonitrile returned uniformly curved nanopillars (Kim et al. 2012).

Effect of Other Parameters

Temperature

A few studies have investigated the role of temperature in MACE. Ultimately, the effect of temperature appears to be the expected one of providing energy to the system with the effect of accelerating its kinetics. Increasing temperature can induce the transition from solid to porous structure (Chen et al. 2010a). Increasing temperature also correlates with higher surface area and larger pores (Loni et al. 2011). Temperatures higher than 50 °C were necessary to obtain porous nanowires from lightly doped n-type silicon in Ag-deposited, H_2O_2/HF etched substrates (Chen et al. 2010a). However, p-type lightly doped porous silicon nanowires have been achieved at room temperature by depositing either Ag or Au (Chiappini et al. 2010; Bai et al. 2012).

It is possible to switch etching from the 100 direction to non-100 direction on both 100 and non-100 substrates by increasing temperature (Kim et al. 2011a; Chen et al. 2010b).

Electric Field

MACE has been combined with electrochemical etch to form localized porous segments in nonporous nanowires and obtain nanowires of prescribed length by cleavage at the porous sections (Kim et al. 2011b). A pulsed current is applied to the substrate to induce periodic porosification. Direct contact to a patterned continuous metal film is necessary to induce localized porosification. If the backside of the wafer is contacted, the entire nanowire structure porosifies upon current pulsing.

Alcohol

Ethanol is typically added to the electrolyte during anodic etch to reduce hydrogen bubble formation, improve pore wettability, and reduce and strain in the resulting layer. Ethanol though is known to differentially affect the activity of

Table 6 Effect of etch parameters on etch rate

Parameter	Action	Effect on etch rate	References
ρ	Decrease	Increase $100 < \rho < 80$	Chartier et al. (2008)
		Decrease $80 < \rho$	
Oxidizer	Increase conc. ~ constant HF	Increase etch rate	Chiappini et al. (2010)
HF	Increase conc. ~ constant H_2O_2	Decrease etch rate	Kim et al. (2011a)
Metal	Ordered by increasing etch rate	$Ag \lesssim Au < Pt < PtPd$	Asoh et al. (2009)
Si resistivity	Increase	Increase etch rate	Chiappini et al. (2010)
Temperature	Increase	Increase etch rate	Chartier et al. (2008), Zhong et al. (2011)
Illumination	Increase intensity	Increase etch rate	Huang et al. (2010b)
Alcohol	Increase conc.	Decrease etch rate	Chiappini et al. (2010)

fluoride ions which is posed to impact the etch outcome. Addition of ethanol to an H_2O_2/HF etching solution induces a progressive change in morphology from solid nanowires, to mesoporous nanowires, to porous silicon layers, and eventually to electropolished structures (Chiappini et al. 2010). Similarly, addition of methanol increased the surface area of porous silicon microparticles synthesized by MACE (Loni et al. 2011). This effect was attributed to foam reduction and improved wetting but could also partially be due to the changes in the etch process associated with alcohol addition. Ethanol was also shown to improve film uniformity in metal-assisted stain etch, while the addition of a tertiary alcohol in the same conditions resulted in a significant decrease in etch rate (Nahidi and Kolasinski 2006).

Etch Rate

Etch rate is an important parameter in MACE not only because it determines the depth of the etch but also because it directly affects the resulting nanostructures. Increasing etch rate has been shown to induce a switch from etching in the <100> direction to etching in the non-<100> direction, for substrates of (100), (110), and (111) orientations (Kim et al. 2011a). Etch rate is tightly correlated with the structure of the porous nanowires (Chiappini et al. 2010). When the etch rate is slower than the rate of porosification, vertical nanowires with vertically aligned mesopores form, often over a layer of porous silicon. When the etch rate is slower than the porosification rate, mesopores are oriented from the sidewalls of the wire toward their core, and partially porous structure can form. The following table summarizes how various known parameters affect etch rate. The table disregards extreme conditions (usually at very high etch rates or for very long etch times) where tip shortening or polishing occurs that effectively reduces the length of the resulting structure and complicates the estimate (Table 6).

Properties of MACE Porous Nanowires

Table 7 provides a brief summary of the investigated properties of porous nanowires synthesized by MACE. For the applications listed, the most relevant handbook chapters are "▶ Porous Silicon and Solar Cells," "▶ Porous Silicon and Li-Ion Batteries," and "▶ Photoluminescence of Porous Silicon".

Table 7 Properties of porous nanowires synthesized by MACE and their field of applicability

Property	Observation	Applicability	References
Reflectance	Dense nanowire arrays show 0.01–3 % reflectance in the 300–800 nm range	Photovoltaics Antireflective coatings	Wang et al. (2012), Sun et al. (2011), Najar et al. (2012)
	Solar-weighted reflectance (4–1.96 %). Decreases with decreasing incidence angle (60°–0°), increasing density of wires, increasing etching temperature, and increasing HF concentration during etch	Photovoltaics	Yeo et al. (2013)
Transmittance	Thin films show increase of high-angle scattering for wavelengths >1 μm	Photovoltaics	Kato et al. (2013)
Wetting	H-terminated wires superhydrophobic (>135°)	Surface coatings	Wang et al. (2012)
	Oxidized wires are superhydrophilic (<5°)		
	Contact-angle dependence on wire density, diameter, length		
In situ PL	H-terminated 525 and 424 nm em	Nanophotonics Optoelectronics	Zhu et al. (2011)
	885 nm em H-terminated	Nanophotonics Optoelectronics	Voigt et al. (2011)
Effect of oxidation on PL	Blue shift of peak with oxidation, with peak intensity increase	Nanophotonics Optoelectronics	Zhu et al. (2011)
	Red shift of peak with oxidation, similar intensity	Nanophotonics Optoelectronics	Voigt et al. (2011)
PL excitation and emission peaks	560 nm emission with 470 nm excitation	Nanophotonics Optoelectronics	Chen et al. (2010a)
	680 nm emission with 442 nm excitation	Nanophotonics Optoelectronics	Qu et al. (2011)

(*continued*)

Table 7 (continued)

Property	Observation	Applicability	References
	590 nm emission	Nanophotonics Optoelectronics	Li and Bohn (2000)
	650 nm emission with 473 nm excitation	Nanophotonics Optoelectronics	Zhang et al. (2009)
PL intensity	Increase PL intensity and energy with increasing etch duration	Nanophotonics Optoelectronics	Voigt et al. (2011), Lin et al. (2010)
	Increase PL intensity and energy with increasing H_2O_2 during etch	Nanophotonics Optoelectronics	Voigt et al. (2011), Lin et al. (2010), Zhang et al. (2013)
Multiple PL sources	Multicolor PL from porous nano-barcodes	Biolabelling	Chiappini et al. (2010)
Transistor fabrication	FET device fabricated from 8 to 13 Ω-cm p-Si, on-off current ratio 10^4, $\mu_h = 46$ cm^2/V, $n = 8.6\ 10^{13}\ cm^{-3}$	Electronics	Zhang et al. (2008)
Conductivity	Threefold increase in conductance for mNW over sNW for lightly doped NW	Nanoelectronics	Chen et al. (2010a)
	mNWs have greatly reduced conductivity over sNW for highly doped NW	Nanoelectronics	Zhang et al. (2009)
Conduction mechanism	Poole-Frenkel conduction	Nanoelectronics	Weisse et al. (2012)
Energy storage	Li storage capacity 2,172 mA h g^{-1}	Li batteries anodes	Wang and Han (2010)
Photocurrent generation	910 μ A/cm^2 photocurrent at 0.2 V bias	Photoelectrochemistry	Wu et al. (2012b)
Toxin degradation	Pt-loaded mNWs degrade indigo carmine (87 %) and 4-nitrophenol (66 %) under light	Photocatalysis	Qu et al. (2010)
	mNWs degrade methyl red (89 %) under visible light	Photocatalysis	Wang et al. (2011)
Thermal conductivity (k)	k decreases with increasing porosity	Nanoelectronics Nanophononics	(Weisse et al)
Inelastic scattering	Ag-covered nanoneedles provide enhanced Raman signal	Surface-enhanced Raman scattering	Kiraly et al. (2013)
Substrate quality	MACE improves metallurgical silicon purity from 99.7 % to 99.9 %	Photovoltaics	Li et al. (2013)

References

Asoh H, Arai F, Ono S (2009) Effect of noble metal catalyst species on the morphology of macroporous silicon formed by metal-assisted chemical etching. Electrochim Acta 54:5142–5148

Bai F et al. (2012) One-step synthesis of lightly doped porous silicon nanowires in HF/$AgNO_3$/H_2O_2 solution at room temperature. J Solid State Chem

Balasundaram K et al (2012) Porosity control in metal-assisted chemical etching of degenerately doped silicon nanowires. Nanotechnology 23:305304

Chartier C, Bastide S, Lévy-Clément C (2008) Metal-assisted chemical etching of silicon in HF–H_2O_2. Electrochim Acta 53:5509–5516

Chen C-Y, Wu C-S, Chou C-J, Yen T-J (2008) Morphological control of single-crystalline silicon nanowire arrays near room temperature. Adv Mater 20:3811–3815

Chen H et al (2010a) Lightly doped single crystalline porous Si nanowires with improved optical and electrical properties. J Mater Chem 21:801–805

Chen H, Wang H, Zhang X-H, Lee C-S, Lee S-T (2010b) Wafer-scale synthesis of single-crystal zigzag silicon nanowire arrays with controlled turning angles. Nano Lett 10:864–868

Chiappini C, Liu X, Fakhoury JR, Ferrari M (2010) Biodegradable porous silicon barcode nanowires with defined geometry. Adv Funct Mater 20:2231–2239

Dimova-Malinovska D, Sendova-Vassileva M, Tzenov N, Kamenova M (1997) Preparation of thin porous silicon layers by stain etching. Thin Solid Films 297:9–12

Douani R, Si-Larbi K, Hadjersi T, Megouda N, Manseri A (2008) Silver-assisted electroless etching mechanism of silicon. Phys Stat Sol (a) 205:225–230

Dudley ME, Kolasinski KW (2009) Stain etching with Fe(III), V(V), and Ce(IV) to form microporous silicon. Electrochem Solid-State Lett 12:D22

Geyer N et al (2012) Model for the mass transport during metal-assisted chemical etching with contiguous metal films as catalysts. J Phys Chem C 116:13446–13451

Harada Y, Li X, Bohn PW (2001) Catalytic amplification of the soft lithographic patterning of Si. Nonelectrochemical orthogonal fabrication of photoluminescent porous Si pixel arrays. J Am Chem Soc 123:8709–8717

Hochbaum AI, Gargas D, Hwang YJ, Yang P (2009) Single crystalline mesoporous silicon nanowires. Nano Lett 9:3550–3554

Huang Z et al (2010a) Oxidation rate effect on the direction of metal-assisted chemical and electrochemical etching of silicon. J Phys Chem C 114:10683–10690

Huang Z, Geyer N, Werner P, de Boor J, Gösele U (2010b) Metal-assisted chemical etching of silicon: a review. Adv Mater 23:285–308

Kato Y, Adachi S (2011) Synthesis of Si nanowire arrays in AgO/HF solution and their optical and wettability properties. J Electrochem Soc 158:K157–K163

Kato S et al (2013) Optical assessment of silicon nanowire arrays fabricated by metal-assisted chemical etching. Nanoscale Res Lett 8:216

Kim J et al (2011a) Au/Ag bilayered metal mesh as a Si etching catalyst for controlled fabrication of Si nanowires. ACS Nano 5:3222–3229

Kim J, Rhu H, Lee W (2011b) A continuous process for Si nanowires with prescribed lengths. J Mater Chem 21:15889–15894

Kim Y, Tsao A, Lee DH, Maboudian R (2012) Solvent-induced formation of unidirectionally curved and tilted Si nanowires during metal-assisted chemical etching. J Mater Chem C 1:220–224

Kiraly B, Yang S, Huang TJ (2013) Multifunctional porous silicon nanopillar arrays: antireflection, superhydrophobicity, photoluminescence, and surface-enhanced Raman scattering. Nanotechnology 24:245704

Kolasinski KW (2005) Silicon nanostructures from electroless electrochemical etching. Curr Opin Solid State Mater Sci 9:73–83

Lee C-L, Tsujino K, Kanda Y, Ikeda S, Matsumura M (2008) Pore formation in silicon by wet etching using micrometre-sized metal particles as catalysts. J Mater Chem 18:1015
Li X, Bohn PW (2000) Metal-assisted chemical etching in HF/H[sub 2]O[sub 2] produces porous silicon. Appl Phys Lett 77:2572–2574
Li X et al (2013) Upgraded silicon nanowires by metal-assisted etching of metallurgical silicon: a new route to nanostructured solar-grade silicon. Adv Mater 25:3187–3191
Lin L, Guo S, Sun X, Feng J, Wang Y (2010) Synthesis and photoluminescence properties of porous silicon nanowire arrays. Nanoscale Res Lett 5:1822–1828
Loni A et al (2011) Extremely high surface area metallurgical-grade porous silicon powder prepared by metal-assisted etching. Electrochem Solid-State Lett 14:K25
Megouda N, Hadjersi T, Piret G, Boukherroub R, Elkechai O (2009) Au-assisted electroless etching of silicon in aqueous HF/H_2O_2 solution. Appl Surf Sci 255:6210–6216
Mikhael B et al (2011) New silicon architectures by gold-assisted chemical etching. ACS Appl Mater Interfaces 3:3866–3873
Nahidi M, Kolasinski KW (2006) Effects of stain etchant composition on the photoluminescence and morphology of porous silicon. J Electrochem Soc 153:C19
Najar A, Charrier J, Pirasteh P, Sougrat R (2012) Ultra-low reflection porous silicon nanowires for solar cell applications. Opt Expr, 20:16861–16870
Peng K, Zhu J (2003) Simultaneous gold deposition and formation of silicon nanowire arrays. J Electroanal Chem 558:35–39
Peng K, Zhu J (2004) Morphological selection of electroless metal deposits on silicon in aqueous fluoride solution. Electrochimica Acta, 49:2563–2568
Peng K, Yan Y, Gao S, Zhu J (2003) Dendrite-assisted growth of silicon nanowires in electroless metal deposition. Adv Funct Mater 13:127–132
Peng K et al (2005) Uniform, axial-orientation alignment of one-dimensional single-crystal silicon nanostructure arrays. Angew Chem Int Ed 44:2737–2742
Peng K et al (2006a) Metal-particle-induced, highly localized site-specific etching of Si and formation of single-crystalline Si nanowires in aqueous fluoride solution. Chem A Eur J 12:7942–7947
Peng KQ et al (2006b) Fabrication of single-crystalline silicon nanowires by scratching a silicon surface with catalytic metal particles. Adv Funct Mater 16:387–394
Qu Y et al (2010) Photocatalytic properties of porous silicon nanowires. J Mater Chem 20:3590
Qu Y, Zhou H, Duan X (2011) Porous silicon nanowires. Nanoscale 3:4060–4068
Sivakov V, Voigt F, Hoffmann B, Gerliz V, Christiansen S Wet-chemically etched silicon nanowire architectures: formation and properties, Nanowires Fundamental Resources, doi:10.577216736
Sivakov V et al (2009) Silicon nanowire-based solar cells on glass: synthesis, optical properties, and cell parameters. Nano Lett 9:1549–1554
Sivakov VA et al (2010) Realization of vertical and zigzag single crystalline silicon nanowire architectures. J Phys Chem C 114:3798–3803
Sun X et al (2011) Fabrication and characterization of polycrystalline silicon nanowires with silver-assistance by electroless deposition. Appl Surf Sci 257:3861–3866
Tsujino K, Matsumura M (2005) Helical nanoholes bored in silicon by wet chemical etching using platinum nanoparticles as catalyst. Electrochem Solid-State Lett 8:C193
Tsujino K, Matsumura M (2007) Morphology of nanoholes formed in silicon by wet etching in solutions containing HF and H_2O_2 at different concentrations using silver nanoparticles as catalysts. Electrochim Acta 53:28–34
Voigt F et al (2011) Photoluminescence of samples produced by electroless wet chemical etching: between silicon nanowires and porous structures. Phys Status Solidi A 208:893–899
Wang XL, Han WQ (2010) Graphene enhances Li storage capacity of porous single-crystalline silicon nanowires. ACS Appl Mater Interfaces 2:3709–3713
Wang F-Y et al (2011) Highly active and enhanced photocatalytic silicon nanowire arrays. Nanoscale 3:3269–3276

Wang W, Li D, Tian M, Lee Y-C, Yang R (2012) Wafer-scale fabrication of silicon nanowire arrays with controllable dimensions. Appl Surf Sci 258:8649–8655

Weisse JM et al. Thermal conductivity in porous silicon nanowire arrays. Nanoscale Res Lett 7:554

Weisse JM, Lee CH, Kim DR, Zheng X (2012) Fabrication of flexible and vertical silicon nanowire electronics. Nano Lett 12:3339–3343

Wu S-L, Zhang T, Zheng R-T, Cheng G-A (2012a) Facile morphological control of single-crystalline silicon nanowires. Appl Surf Sci 258:9792–9799

Wu S-L, Zhang T, Zheng R-T, Cheng G-A (2012b) Photoelectrochemical responses of silicon nanowire arrays for light detection. Chem Phys Lett 538:102–107

Yae S, Kawamoto Y, Tanaka H, Fukumuro N, Matsuda H (2003) Formation of porous silicon by metal particle enhanced chemical etching in HF solution and its application for efficient solar cells. Electrochem Commun 5:632–636

Yae S, Tanaka H, Kobayashi T, Fukumuro N, Matsuda H (2005) Porous silicon formation by HF chemical etching for antireflection of solar cells. Phys Stat Sol (c) 2:3476–3480

Yae S et al (2007) Nucleation behavior in electroless displacement deposition of metals on silicon from hydrofluoric acid solutions. Electrochim Acta 53:35–41

Yeo C, Kim JB, Song YM, Lee YT (2013) Antireflective silicon nanostructures with hydrophobicity by metal-assisted chemical etching for solar cell applications. Nanoscale Res Lett 8:159

Zhang ML et al (2008) Preparation of large-area uniform silicon nanowires arrays through metal-assisted chemical etching. J Phys Chem C 112:4444–4450

Zhang C et al (2009) Electrically conductive and optically active porous silicon nanowires. Nano Lett 9:4539–4543

Zhang C et al (2013) Enhanced photoluminescence from porous silicon nanowire arrays. Nanoscale Res Lett 8:277

Zhong X, Qu Y, Lin Y-C, Liao L, Duan X (2011) Unveiling the formation pathway of single crystalline porous silicon nanowires. ACS Appl Mater Interfaces 3:261–270

Zhu M et al (2011) Structural and optical characteristics of silicon nanowires fabricated by wet chemical etching. Chem Phys Lett 511:106–109